STRUCTURAL FAULTS + REPAIR – 2006

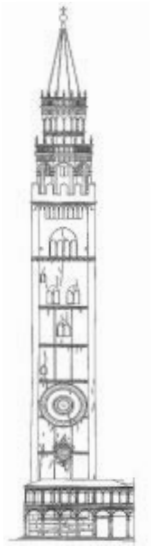

11th International Conference and Exhibition

13th – 15th June 2006

Assembly Rooms
George Street

Edinburgh, Scotland

Innovation in "Extending the Life of Bridges, Concrete + Composites, Buildings, Masonry + Civil Structures"

3 Themes each spread over 3 days

• 3-Day Registration at £430 stg • Daily Registration at £215 stg per day

200+ Papers from 37 Countries

Theme 1	:	BRIDGE INVESTIGATION AND REPAIR
Theme 2	:	CONCRETE + COMPOSITES IN REPAIR
Theme 3	:	BUILDINGS, MASONRY + CIVIL STRUCTURES

EXHIBITION @ STRUCTURAL FAULTS + REPAIR – 2006

Early Exhibition bookings:

Allied Associates Geophysical
Amphora NDT Limited
Aperio Limited
Brookes Specialist Contractors Limited
Cintec International Limited
City University
Contec International Products Ltd
CNS Farnell
Concrete
Concrete Engineering International
Elsevier Ltd
Freyssinet Limited

Geophysical Survey Systems Inc (Gssi)
Helifix Ltd
Hemming Information Services

Heriot-watt University
Hilti Corporation
Holequest Ltd
Holroyd Instruments Ltd
Inspectahire Instrument Co Ltd
Physical Acoustics Ltd
Queens University - Belfast
Sengenia Measurements Ltd
Sensors & Software Inc
Strainstall Uk Ltd
Taylor Woodrow Technology
University Of Edinburgh
Weber Building Solutions

www.structuralfaultsandrepair.com – Tel: 0131–447 0447

RADAR INVESTIGATION ON CIVIL STRUCTURES USING 3D DATA RECONSTRUCTION AND TRANSMISSION TOMOGRAPHY

Lukasz Topczewski, Francisco Fernandes, Paulo J.S. Cruz, Paulo B. Lourenço, Luís F. Ramos
University of Minho
Department of Civil Engineering
4800-058 Guimarães
Portugal
lukasz@civil.uminho.pt

KEYWORDS: NDT, GPR, 3D reconstruction, Tomography, Concrete, Masonry.

ABSTRACT
Non-destructive investigation using Ground Penetrating Radar is becoming more popular during the inspection of civil structures. Currently, traditional 2D imaging is also used as a preliminary tool to find possible areas of interest for more detailed inspection, which can be accomplished by 3D image reconstruction or tomography techniques. In this paper, a general overview of the work done at University of Minho regarding these techniques is presented. Data acquisition was performed on two masonry walls and on one large concrete specimen. In case of masonry specimens traditional 2D imaging was supplemented by the use of transmission tomography. Data acquisition on the concrete specimen was done in reflection mode and results were further processed using 3D reconstruction software.

Results from these specimens are very promising. Radar tomography and 3D image reconstruction techniques provided much more detailed information about structural integrity and shapes and location of the voids placed inside the tested specimens relatively to 2D imaging originally used for potential target identification.

INTRODUCTION

Exhaustive preliminary inspections using non-destructive inspection techniques (NDT) are becoming rather common in restoration and retrofitting projects as well as within maintenance programs of civil structures. A widely known NDT technique is the Ground Penetrating Radar (GPR). Such technique is very attractive due to the possibility to reliably acquire non-visible information without causing damages to the structure, which is becoming a key aspect for the conservation of structures.

Despite the fact that designers and architects are becoming more conscious of the potential of this non-destructive technique, its use is still not frequent outside the academic community. In Portugal, only a few number of investigation institutes possess such equipment.

In this paper, the authors wished to contribute to the increase of the use of GPR by showing two examples where the detection capabilities of GPR with high frequency antennas and advanced software and acquisition techniques were successfully used to detect and diagnose common problems in concrete and masonry structures. The main techniques used in the paper are shortly described in the following section. The experimental part consists of two examples that show the application of such techniques to solve particular problems and its advantages over traditional 2D radargrams.

ADVANCED TECHNIQUES IN GPR FOR IMAGE PROCESSING

GPR is a non-destructive technique based on emission of electromagnetic energy in a vast range of frequencies (25 MHz to 2.2 GHz). Theoretical background and operative modes of GPR have been described in detail by some authors (Daniels, 2004). Radar is used commonly in the reflection mode to collect data by dragging an antenna on the surface. This information results in 2D radargrams, which is the most frequent way of analyzing radar data. For most common problems such as thickness measurements (Krause et al, 1995), rebar detection (Hugenschmidt, 2002), location of large voids (Maierhofer et al,

2003), and in most building materials (masonry and reinforced concrete) this mode reveals to be the most suitable, fastest and cheapest. However, in some particular cases it is not enough. In cases where individual radargrams provide very little information, when they are very difficult to interpret and when the objective are small objects or defective/damaged areas, more advanced techniques can be applied.

One of these techniques consists in obtaining a 3D volume of the radar data by acquiring a dense subset of parallel 2D radar profiles (Valle et al, 2000, Groenenboom et al, 2001). This technique has been successfully applied in numerous applications of NDT investigation of civil structures such as for better visualization of radar data within investigated area by showing the results as depth slices (Lualdi et al, 2003) or by providing more realistic views of the objects through isosurfaces (Binda et al, 2003a). It allows also non-specialized radar users to better understand radar results by providing more realistic shapes of embedded features. In this paper, 3D reconstruction is used for the assessment of common structural elements, faults and defects inside a simulated bridge deck.

The second technique used in this paper is called tomography. Radar tomography is a technique to map the interior of objects like pillars, columns, walls and other elements that can be accessed from two or more sides. An electromagnetic pulse is transmitted on one side and received on another. Either traveltime (velocity tomography) or amplitude (attenuation tomography) information from many transmitter-receiver pairs is used to reconstruct the hidden structure. The specific information about the technique and reconstruction algorithms can be found elsewhere (Valle et al, 1999). This technique can be used generally to map: voids, moisture content and embedded timber elements (Binda et al, 2003b). However due to the high time, hardware and software requirements necessary for acquisition, this technique is still only used to solve localized problems. In this paper, tomography is used to map a wood beam and a polystyrene prism embedded in two stone masonry walls.

ANALYSIS OF DEFECTS IN CONCRETE WITH 3D RECONSTRUCTION

Description of the Test Specimen and Methodology

A concrete specimen has been specially designed and built for this testing campaign in April 2004 aims to simulate a small part of a typical concrete bridge deck. It is a square with dimensions of 250 × 250 cm and a thickness of 32 cm. The elements that were placed inside were chosen among typical elements used in the construction of structural elements in reinforced and pre-stressed concrete bridge decks. A number of typical defects and anomalies that may occur deriving from errors during the construction were put in the specimen as well. A general view of the features inside the slab before being filled with concrete is illustrated in Fig. 1a, while a general view of the final specimen is illustrated in Fig. 1b.

(a) (b)

Fig. 1 General view of the concrete specimen. (a) Overview of the features and objects placed inside the specimen and (b) final view of the slab

Inside the slab were placed three tendon ducts in PVC, one with 110 mm and the other two with 35 mm of diameter. The larger tendon duct is generally used for the introduction of post-tensioning cables, while the two smaller tendon ducts are simulating simple mono-cables, one in straight line and the other with a curved path. The objective is to detect all tubes by radar and to verify if all tubes are correctly detected,

with special attention to the curved tube. The measurements will be performed without cables inside the smaller tubes. However, in the largest one, half the tube is fully grouted with cement grout and the other half only half grouted in order to check the difference between fully filled and partially filled sections in tendon ducts. Several other deficiencies were simulated as well, such as the event of a poorly vibrated or lower density concrete, which was simulated by: blocks of concrete with insufficient binder (poor concrete), different density concrete (light-weight concrete), large voids and blocks with inclined surfaces. Furthermore, one empty bottle, one clay brick, wood and mortar prisms and two metallic bars were also put in this specimen. Additionally, a pre-casted concrete element (class C30/35) was placed at the bottom of the specimen (Fig. 1a) and occupies half of the total area of the slab. The thickness of this element is 7 cm, and the location inside the concrete specimen is illustrated in Fig. 2.

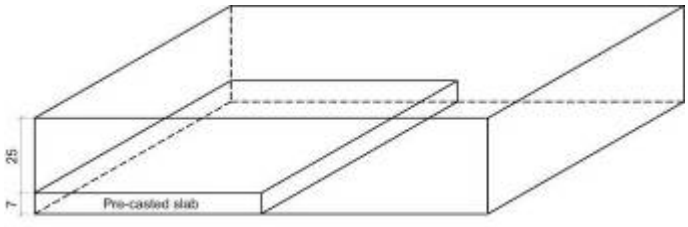

Fig. 2 Location of the pre-casted element inside the concrete specimen.

The rest of the specimen is filled with pre-fabricated concrete (class C30/35). No metallic reinforcement bars were used to build this specimen, only metallic grids were used in the bottom of the specimen and in the upper surface of the pre-casted slab in order to prevent premature cracking and increase the specimen's strength. The grid is constituted by metallic wires with 2 mm of diameter and squared cells with 15 cm of edge. An additional metallic piece was also provided in contact with the pre-casted element in order to be able to easily detect it in the radargrams.

Concerning the GPR system used for the acquisition, the authors used the RAMAC/GPR from MALA Geoscience. The system was equipped with an antenna with a central frequency of 1.6 GHz, which was preferred due to the high resolution it provided and due to the small dimensions of the targets of this investigation. A digital hip-chain was used as positioning system and as pulse trigger.

Moreover, in order to construct good 3D images, longitudinal 2D profiles closely spaced (5 cm apart) were drawn over the areas of interest. Such a density of longitudinal profiles was essential in order to obtain a realistic 3D image and necessary to map all possible elements. In Fig. 3a is illustrated the grid drawn over the surface of the slab. Two areas of interest have been selected and are reported in Fig. 3b: one is constituted by half the specimen (Area 1 in Fig. 3b), where are located most of the deficiencies (poorly vibrated concrete, voids, etc.) and half of the pre-casted slab, and a second one (Area 2 in Fig. 3b) that considers all the area of the specimen, specially the three tendon ducts. Radar acquisition in the area 2 was carried out in the direction perpendicular to the tendon ducts in order to maximize the return of the signal reflected by the tendon ducts. Area 1 was acquired parallel to the tendon ducts, so, the mapping of these elements was not considered.

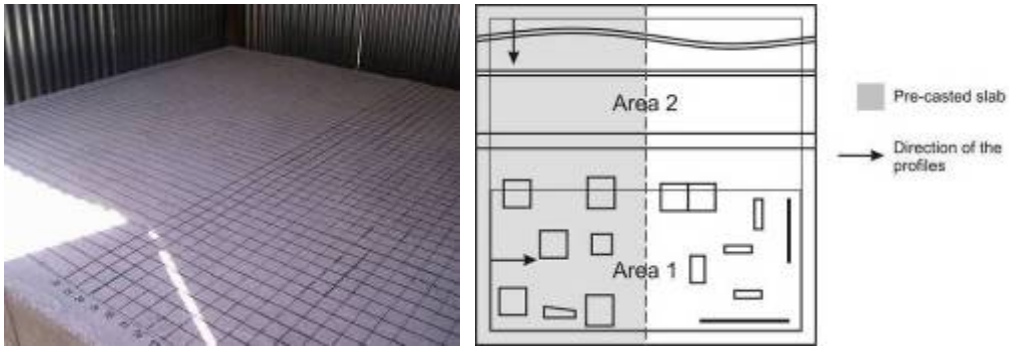

Fig. 3 3D measurements. (a) Partial view of the grid drawn over the surface of the slab and (b) location of the areas of interest.

Results and Discussion

The analysis of the 2D profiles provided depth and location information about the elements located under each profile. Then, all profiles were merged in a 3D volume. Afterwards, it was possible to extract slices at different depths, which provided additional information such as shape and localization of the elements. The first area to be discussed will be Area 1 followed by Area 2, where the results from 3D reconstruction present indeed a clear advantage over 2D profiles in the specific case of bridge deck investigation.

Results from Area 1

The objective in this area was to determine the position and shape of all the elements, position of the opposite surface and the pre-casted slab. In Fig. 4 is illustrated one radargram that shows the opposite surface at 7 ns of depth. The opposite side was detected by means of the hyperbolas reflected by the metallic mesh, which was used to prevent concrete shrinkage, located at the bottom of the slab, almost in direct contact with the surface. As these hyperbolas were considered to correspond to the bottom of the slab, the 7 ns were considered to correspond to the 32 cm of thickness of the slab. This resulted in an average radiowave velocity of 9.2 cm/ns, which is rather low for concrete. Typical velocities in dry concrete are 9-13 cm/ns. The pre-casted slab was detected in the first half of the radargram, at 5 ns from the surface, and a thickness around 1.5-2 ns (6.8-9.1 cm).

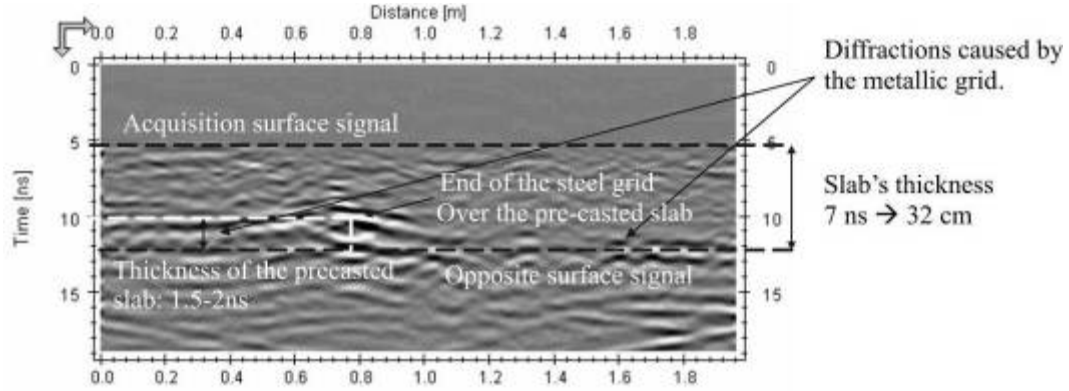

Fig. 4 Detection of the opposite surface of the slab as well as the pre-casted slab.

In Fig. 5 are shown additional profiles from where it is clear that poorly vibrated concrete and voided elements were successfully detected, as well as the metallic bar. From the radargrams below, the length of the concrete elements were acquired with rather satisfactory accuracy (the dashed boxes correspond to the dimensions of those elements). The height computed with the velocity of 9.2 cm/ns resulted in lower values than the real ones, which seem to suggest that the velocity within these concrete elements is slightly higher than in the rest of the whole specimen (radiowaves in porous concrete have a higher velocity than in full concrete). The position of objects is also rather accurate according to the location of two concrete blocks in the 22nd profile, relatively to the center axis. The radargram reported 12.5 cm, while it was located at 12 cm (relatively to design plans). However, one element in each of the profiles from lines 4 and 22 was not detected. It must be noted that these elements have a triangular shape (see Fig. 1a) and that the incident waves in such surfaces are scattered in a direction far from the receiver position. Thus, they are very difficult to detect.

Subsequently, the 3D image was build by performing linear interpolations between successive and closely spaced 2D radargrams. This way, it was possible to obtain a more realistic view of the data and, eventually, to better define the shapes and relative position of the objects previously detected with 2D profiles. The whole data is migrated in order to transform the diffraction hyperbolas in patterns closer to the shape of the objects they represent, and slices at different depths can be extracted to compare with the original design drawings. In Fig. 6 two examples of time slices extracted from the main 3D volume are illustrated. Generally, a good correlation between the dimensions and relative position of single objects with the original design plans was obtained. However, in some cases, their relative position can differ due to deviations caused by the filling of the formwork with concrete and due to the vibration process. On the top radargram of Fig. 6 is illustrated a particular case where the original positions, in white, are different from

the actual position, in black, detected by the antenna. However, not all elements were detected. Relatively to the shape of the objects, it depends exclusively in the effects caused by the migration algorithm, which concentrates energy in the apex of the events. Additionally, the length and the starting point of the profiles were not rigorously the same due to the positioning system used during the acquisition.

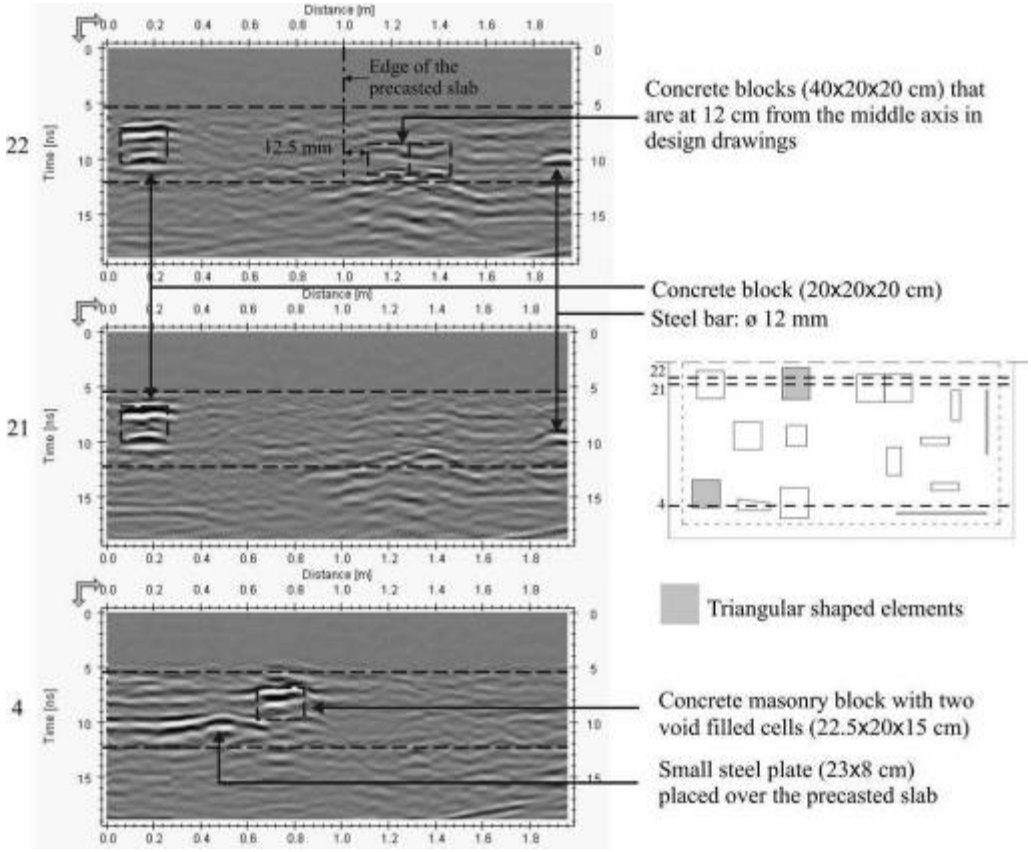

Fig. 5 2D profiles of the 22nd, 21st and 4th acquisition lines, respectively, from top to bottom.

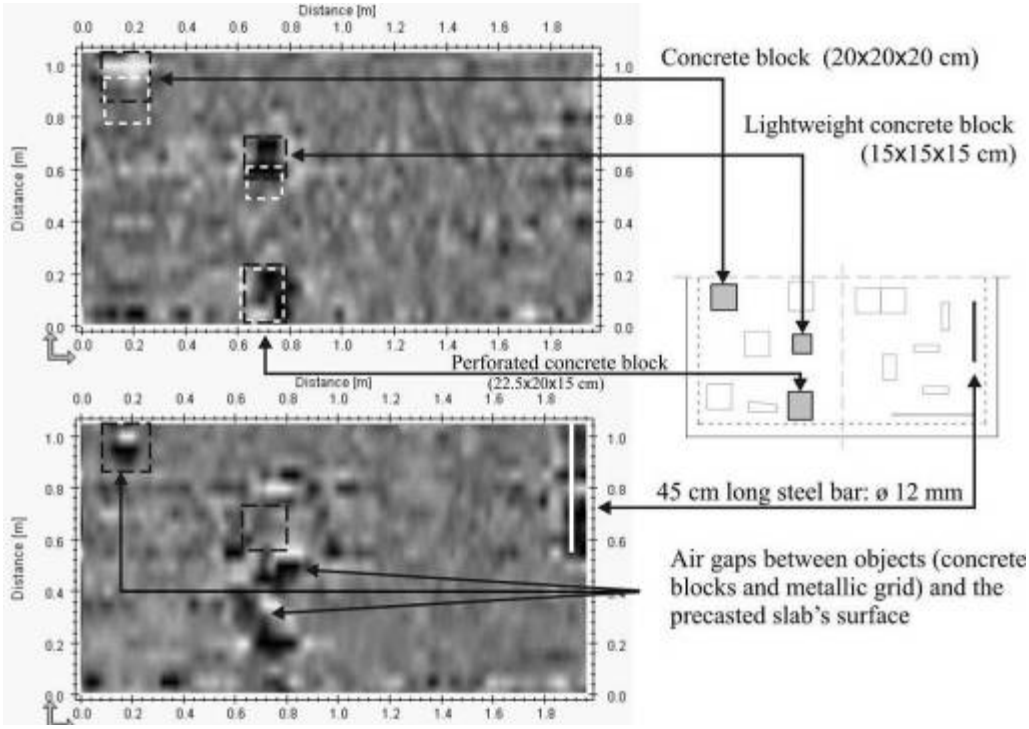

Fig. 6 Time slices from the migrated 3D volume with accurately positioned objects that are not in their original location. Depth of the slices: 10 and 18.5 cm, respectively, from top to bottom.

Results from Area 2

The second area considered for the investigation corresponds to the totality of the slab's surface (see Fig. 3), with the objective of mapping the features located in the interior of the slab. In this case, particular interest lied on the detection of the three tendon ducts, especially in the correct acquisition of the curved shaped tendon duct and in the larger one, which has half and fully grouted sections.

The analysis of the normal 2D profiles showed that the three tendon ducts were detected in all cases. The radargram in Fig. 7 illustrates the three tendon ducts, where it appears that the two smaller diameter tendon ducts (35 mm) are detected by their superior interface, while in the case of the larger diameter tendon duct (110 mm), both interfaces seemed to be detected. This phenomenon is associated to the short wavelength of the 1.6 GHz antenna, which is 18.75 cm, from where it results in an expectable resolution of 47 mm, taken as $\lambda/4$ (Forde, 2004). Because the diameter of the smaller tendon ducts is inferior to 47 mm, the signal from the upper interface of the smaller tendon ducts would cover the lower interface signal, which happens effectively. Only the signals that were reflected by the boundaries of the largest tendon duct are both visible due to the fact that the distance between them is longer than the signal's expected resolution. However, this depends on the contrast between the tendon duct and the infill material (air, grout or steel bar).

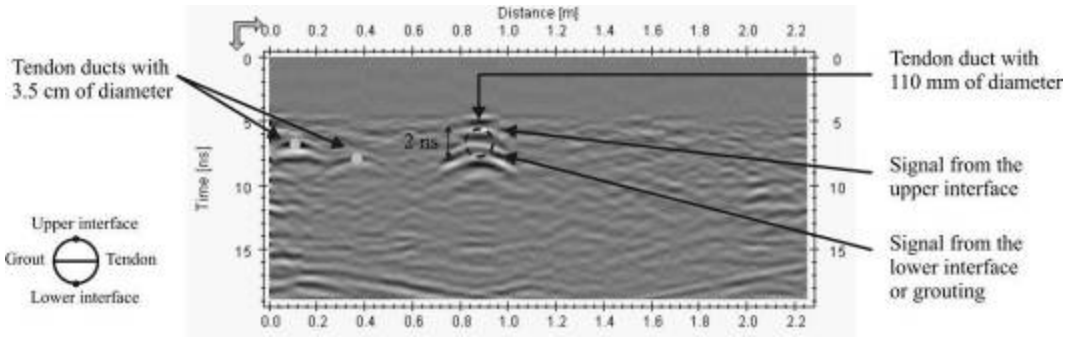

Fig. 7 First profile at 10 cm from the border.

The analysis of the time slices gives good results as it was possible to resolve all intended targets, namely the three tendon ducts, and the position and shape of some of the other targets (not all targets were indeed resolved). In the following radargrams illustrated in Fig. 8 are visible several concrete blocks as well as one of the reinforcement steel bars, the one that was perpendicular to the direction of radar acquisitions. The quadratic/rectangular shape of the objects is quite reasonably detected after the migration of the data. However, some of the objects placed in the interior of the concrete specimen were not exhibited. Most probably, some of them were not detected because they were oriented in parallel to the radar profiles (plastic bottle and clay brick), and others were two small or too deep to be reached by the radiowave (lightweight concrete cube, mortar and wood prisms) as well as lack of contrast (concrete cube with 5 cm of edge).

The mapping of the three tendon ducts is shown in Fig. 9. All ducts were correctly detected and the curvature of the curved duct is well defined. Regarding the largest tendon duct, although it has been correctly detected, the intensity of the signal amplitude is not uniform along its entire length. As it can be seen in the 2nd and 3rd radargrams of Fig. 9, the radiowave's energy seems to be higher in the bottom part of the section, where the tendon duct's section is half grouted. The air in that area could explain the higher energy due to the higher contrast between dielectric constants of concrete ($\varepsilon_{r,\,concrete} = 6$) and air ($\varepsilon_{r,\,air} = 1$), which does not exist between concrete and grout. Thus, it seems possible to detect differently filled tendon ducts sections by analyzing the amplitudes of the reflected signals, although it has shown to be irregular as it can be seen in the first radargram of Fig. 9.

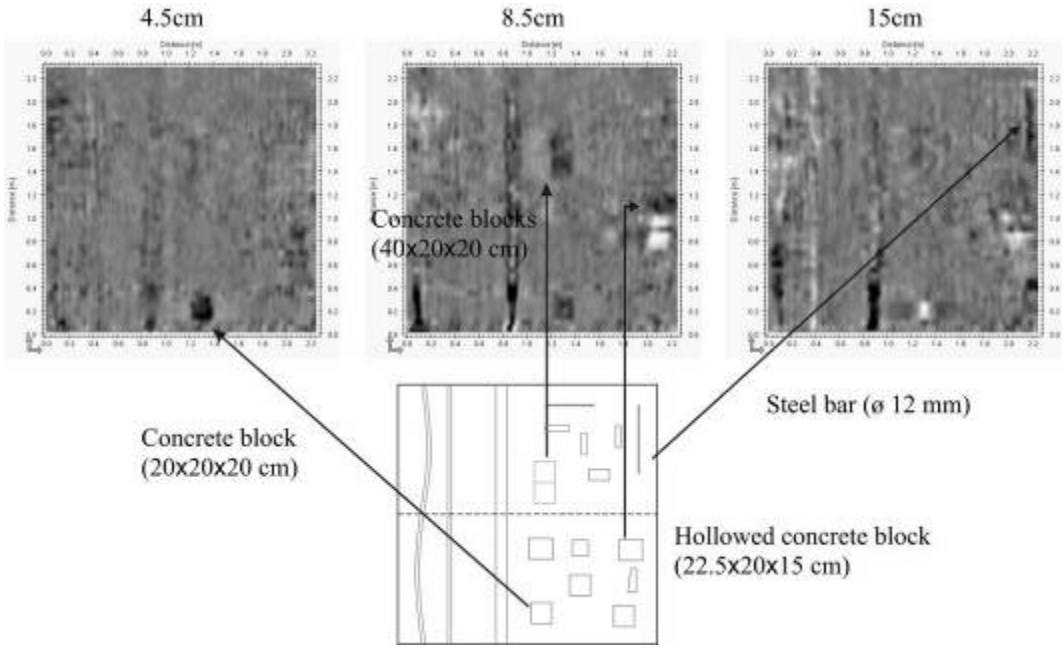

Fig. 8 Time slices after migration where are observed some of the concrete blocks and the steel bar perpendicular to the acquisition direction.

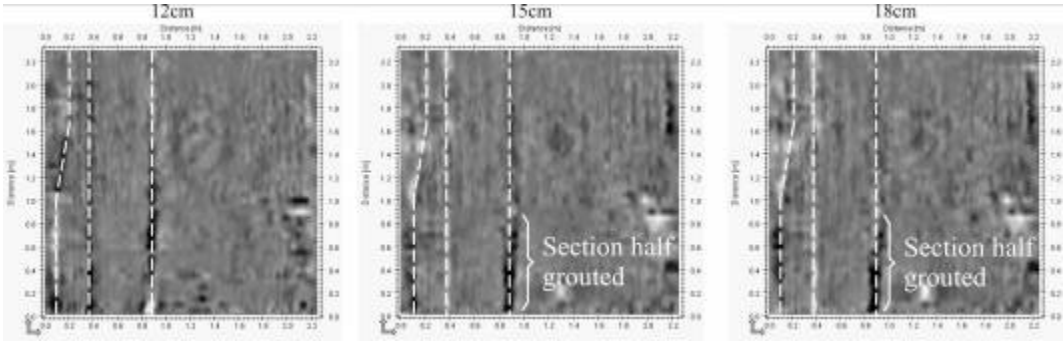

Fig. 9 Radargrams showing the three tendon ducts.

MAPPING OF EMBEDDED ELEMENTS IN MASONRY WALLS WITH TOMOGRAPHY

Description of the Test Specimen and Methodology

The two walls were built with three different masonry typologies with very weak lime mortar in order to simulate different but typical historic masonry typologies (Fig. 10) and two different materials for the infill were used (gravel and stone and brick rubble). Additionally, a void was simulated with a high density polystyrene prism in the first wall and a wood beam was placed in the second wall. Both were placed vertically within the two walls.

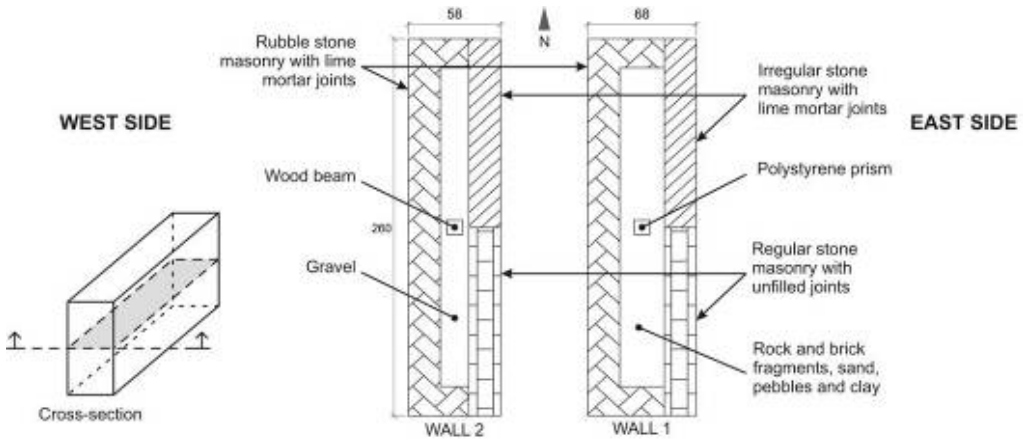

Fig. 10 Horizontal cross-sections of the two masonry walls (cm).

Both walls are made with three-leaves, constructed on top of a small 5 cm thick concrete slab, cast only with the purpose of rectifying the ground surface where the walls were erected. At the top of each wall, a thin layer of concrete was laid in order to protect the interior of the walls from rain and dust. A small slope was provided to facilitate rainwater drainage. The dimensions of the walls are, 122 cm in height by 260 cm in length. The thickness of the eastern wall (*Wall 1*) is 68 cm and 56 cm for the western wall (*Wall 2*). The masonry typology adopted in the walls is constituted, in the western side, by a rubble stone masonry with lime mortar joints, with a thickness of 20 cm. In the eastern side, two different masonry typologies were used: a 20 cm thick panel of regular masonry with unfilled joints and a panel of irregular stone masonry with lime mortar, with an average thickness of 20 cm.

Moreover, for *Wall 1*, the infill was constituted by rock and brick fragments, sand, pebbles and clay, in order to simulate an inhomogeneous infill material of low strength. In *Wall 2*, the infill is made of gravel, with 2-3 cm of diameter and almost no cohesion. The objects embedded in the walls have the following dimensions: high density polystyrene prism: 9.5×8×40 cm (Fig. 11c), wood beam: 6.5×6.5×100 cm (Fig. 11b). The objectives of the present investigation were to distinguish the different layers and to detect the wood and polystyrene elements placed inside the walls.

Fig. 11 View of the embedded objects. (a) Polystyrene prism. (b) Wood beam.

Results and Discussion of 2D acquisitions (target location)

The investigation on the two masonry walls was carried out with the RAMAC/GPR system from MALA Geoscience. A 1.6 GHz frequency antenna was used for all measurements, and a digital hip chain was used as triggering and positioning device system. This configuration was preferred over the survey wheel due to the irregularity of the surface. The average radiowave velocity was assessed with the antenna in the centre of the masonry panels oriented towards east and a steel plate placed over the opposite surface. The acquisition in time resulted in an average radiowave velocity around 12.0 cm/ns in both walls.

Several horizontal profiles were carried out on the eastern sides of both walls (with two panels of regular and irregular masonry). The centre of the antenna started at 15 cm of the edge and ended at 10 cm from the extremity. This resulted in profiles with a length of 225-230 cm. The horizontal profiles were separated by 5 cm.

Fig. 12 represents a radargram from *Wall 1* in the upper part of the wall. The data has been filtered and a gain function was applied to enhance the diffractions. It is possible to recognize the regular masonry panel by the horizontal signal it has produced at the beginning of the profile (at 3.5 ns), while the second panel is detected via the hyperbolas that spread in the first nanoseconds. The interface between the first leaf and the infill material was clearly defined at an average depth of 3.5 ns, characterized by a strong reflection due to air voids caused by the deficient contact between stone and infill. The construction of these walls followed a traditional way, thus, no compaction was done to the infill, with the consequence of a high probability of occurrence of voids. Taking the velocity found earlier (12 cm/ns) the final thickness of the stone layer was estimated in 21 cm (error of 5 % relatively to the design thickness). However, the no clear radargram was obtained showing clearly the signal from the polystyrene prism.

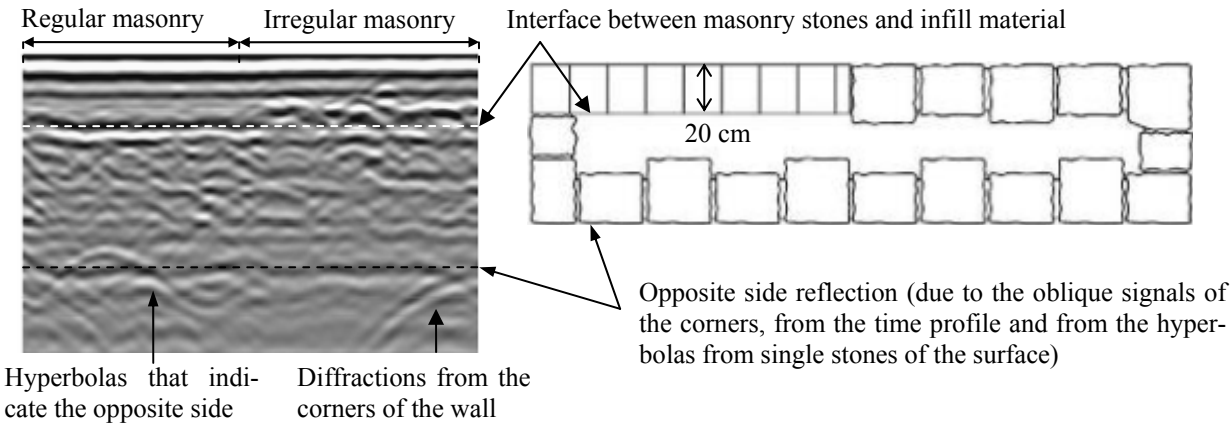

Fig. 12 Ninth profile on *Wall 1* at 49 cm with the 1.6 GHz antenna.

With respect to *Wall 2*, the interface between the first stone panel was detected (see Fig. 13a), with a clear distinction between regular and irregular masonry, at 100-110 cm from the beginning of the profile. Afterwards, the irregularity of the signal indicates an irregular interface that corresponds to the irregular masonry panel. The wood beam placed within the infill was correctly detected by a rather strong diffraction at ≈ 110 cm from the beginning of the profile. A slight error was observed then when comparing this value to the original design position. The signal from the opposite surface was detected. However, the second interface (infill/masonry) was not detected.

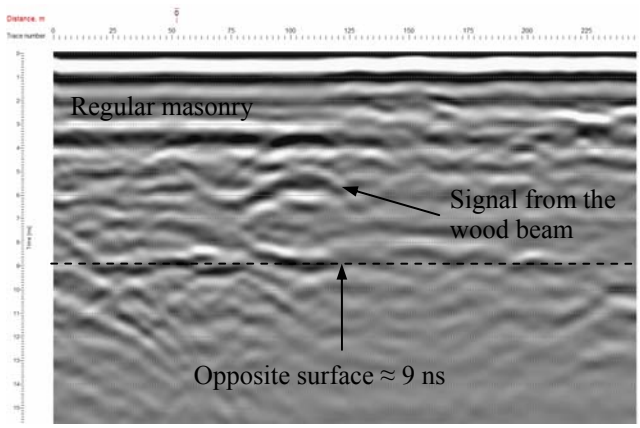

Fig. 13 Radargram at 29 cm from the concrete base with the 1.6 GHz antenna.

Results and Discussion of tomography (target mapping)

2D reflection radargrams were extremely useful in the detection and location of the timber beam and the polystyrene prism embedded in the two masonry walls. However, in order to assess the nature and the shape of these objects, transmission measurements will be carried out in the area where those objects were detected. Transmission measurements result in velocity and attenuation tomograms that can help to identify the nature and shape of the embedded elements. This topic is currently being developed and improved in the frame of the European project Sustainable Bridges.

The measurements were carried out in both walls with two 1.6 GHz antennas. The investigation area was selected around the location of the embedded elements that were estimated from the 2D radargrams. With respect to *Wall 1* (with the polystyrene prism), the section of interest was located 40 cm below the top of the wall and consisted in an area of 100×68 cm^2 illustrated in Fig. 14. The transmitter was sequentially fixed in eleven stations separated by 10 cm, while the receiver was performing eleven continuous profiles in the opposite side of the wall. WinTomo software (proprietary of MALA Geoscience) was used to process the radar data and to obtain the final velocity and attenuation tomograms.

The final velocity tomogram obtained from the investigation in *Wall 1* is illustrated in Fig. 14. It shows that the major part of the tomogram exhibits an average velocity smaller than 12 cm/ns. The borders of the tomogram are characterized by a substantial number of artefacts and other side effects, which were not taken into consideration. A small area exhibiting a very high velocity, around 18 cm/ns, is located in the centre of the tomogram. Its position corresponds to the position of the polystyrene prism. From the tomogram can be perceived that the speed of propagation of radiowaves within polystyrene is close to the velocity in air (which is why this material is often used for air substitution when simulating air voids inside structures). The area with high velocity radiowaves correspond to an area 19 % smaller than the area of the polystyrene prism.

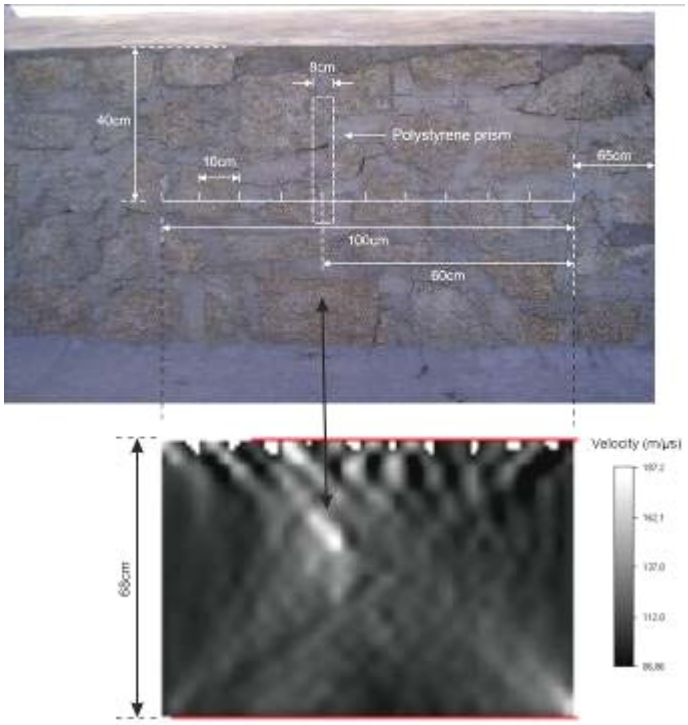

Fig. 14 Tomography in *Wall 1*. (a) Position of the fixed stations for the transmitter antenna and relative position of the polystyrene prism in the grid of measurements. (b) Velocity tomogram.

With respect to *Wall 2* (with the wood beam), the section of interest was located 30 cm below the top of the wall and consisted in an area of 80×58 cm^2 illustrated in Fig. 15. The transmitter was sequentially fixed in nine stations separated by 10 cm, while the receiver was performing nine continuous profiles in the opposite side of the wall. The final velocity tomogram obtained from the investigation in *Wall 2* is illustrated in Fig. 15. The major part of the tomogram exhibits an average velocity around 14 cm/ns. The area that was interpreted as being from the wood beam correspond well to its geometrical location and exhibits a very high velocity, around 19 cm/ns, slightly higher than in polystyrene, which reveals that the radiowave velocity is similar in both materials. However, the borders and interior of the tomogram are characterized by a substantial number of artefacts and other side effects that affect quite severely the quality of the data. In this case, the resolution of the tomogram is much limited due to the reconstruction algorithms used by the software. This problem has already been described by other authors (Valle et al, 1999).

To complement this result, a second tomogram is showed in Fig. 16. This tomogram represents the distribution of signal amplitudes across the cross-section of the wall and allows to find areas where low attenuation of the signal occurred. In this case, dark areas correspond to areas where the signal's amplitude suffered low attenuation. A dark spot corresponds to the position of the wood beam, which means that the signal experiences low attenuation when propagating through wood.

The area of the wood beam cross-section was estimated from both tomograms but results were rather distinct. While in the first case (Fig. 15) the area in the tomogram was 17 % larger than the real area of the

wood beam, in the second case (Fig. 16), the area was estimated 19 % smaller than the real area of the wood beam.

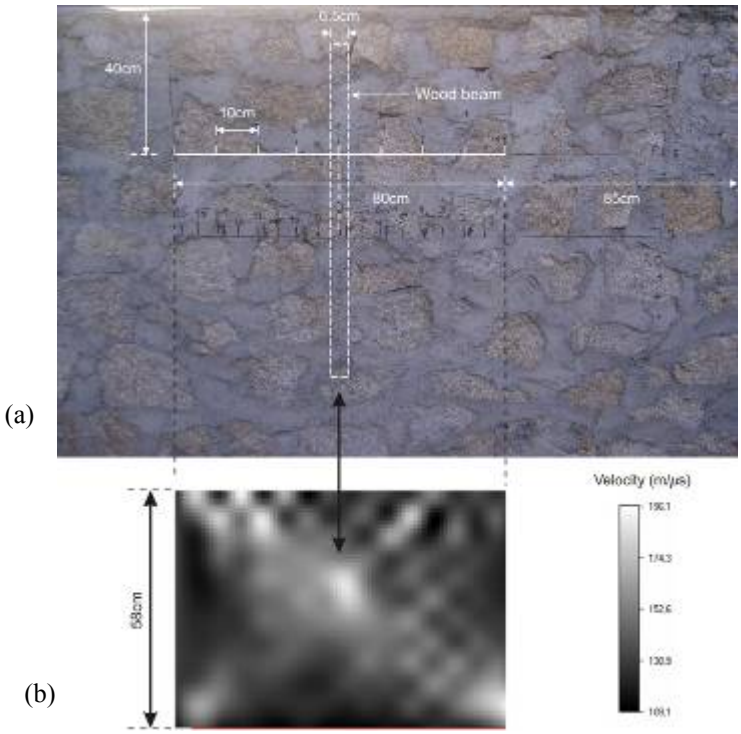

(a)

(b)

Fig. 15 Tomography in *Wall 2*. (a) Position of the fixed stations for the transmitter antenna and relative position of the polystyrene prism in the grid of measurements. (b) Velocity tomogram.

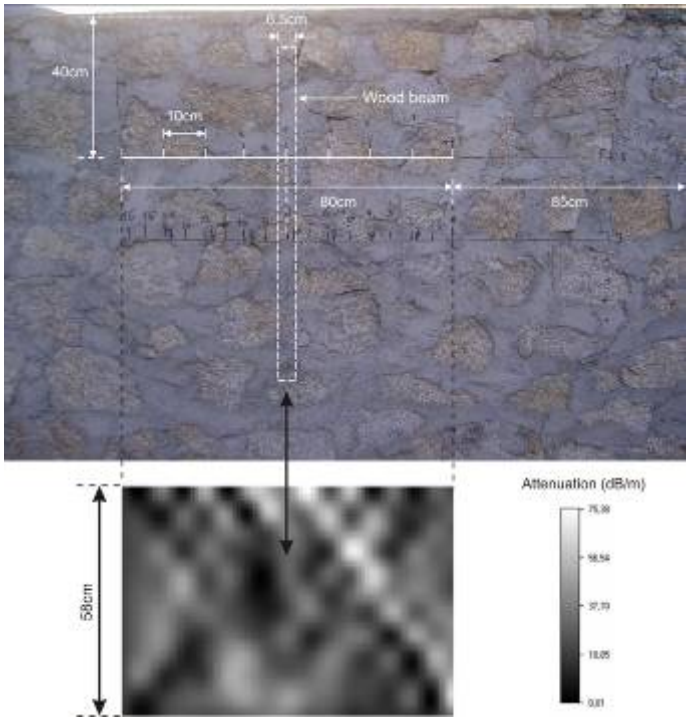

(a)

(b)

Fig. 16 Tomography in *Wall 2*. (a) Position of the fixed stations for the transmitter antenna and relative position of the polystyrene prism in the grid of measurements. (b) Attenuation tomogram.

CONCLUSIONS

The use of GPR with 3D reconstruction showed good potential in the detection of the main structural elements as well as with the mapping of typical deficiencies frequently found in concrete structures within large areas. The tendon ducts were all detected and the curvature of the curved tendon duct was

correctly assessed. The antenna with a central frequency of 1.6 GHz exhibited very good resolution and high accuracy.

However, not all targets were resolved, but the analysis pointed out several reasons to explain these results. Effectively, some of the targets were not detected due to its unfavorable orientation relatively to the direction of the profiling, which was the case of all objects parallel to the profiles. Because the profiles started and ended 10-15 cm after and before the specimen's border, some objects located very close to the edges of the specimen were not detected as well. Particularly the steel bar perpendicular to the tendon ducts. Moreover, the poor contrast between materials resulted in poor reflectivity and thus weak detection, particularly in the case of the lightweight concrete specimen. Additionally, the triangular shapes did not reflect favorably for detection by the radar signals, which resulted in the non detection of those objects.

Radar tomography used for target assessment subsequent to target detection by reflection mode showed to be a good combination. With respect to the detection capabilities of this configuration, the wood beam was clearly detected and the position was found to be different from the expected one. The tomography carried out in both walls resulted in satisfactory results, and both polystyrene prism and wood beam were located. However, this methodology was limited by the significant number of artifacts that appeared in the final results that masked partially the targets of the investigation, especially in the case of the wood beam.

The results showed good potential for the described applications, but there is still need to improve positioning systems for more accurate acquisitions and improved software tomography algorithms and signal processing.

ACKNOWLEDGMENTS
The first author would like to acknowledge the support from "Sustainable Bridges" European project by the grant number FP6-PLT-01653. The second author would like to acknowledge the partial support from FCT (Portuguese Foundation for the Science and Technology) by the grant number POCTI SFRH/BD/6409/2001.

REFERENCES

- Binda, L., Lualdi, M., Saisi, A., Zanzi, L., Gianinetto, M. and Roche, G. (2003a), "NDT applied to the diagnosis of historic buildings: a case history," *Proc., Structural Faults & Repair*, London, UK, 10p.
- Binda, L., Saisi, A., Tiraboschi, C., Valle, S., Colla, C. and Forde, M. (2003b), "Application of sonic and radar tests on the piers and walls of the Cathedral of Noto," *Construction and Building Materials*, Vol. 17, No. 8, 613-627.
- Daniels, D.J. (2004), *Ground Penetrating Radar - 2nd Edition,* Radar, sonar, navigation and avionics series 15, IEE, London, UK, ISBN 0-86341-360-9, 726p.
- Forde, M.C. (2004), "Ground Penetrating Radar," *Proc., Introduction to Non-destructive Evaluation Technologies for Bridges Conference*, Transportation Research Board, 20p.
- Groenenboom, J., Van Der Kruk, J. and Zeeman, J.H. (2001), "3D GPR data acquisition and the influence of positioning errors on image quality," *Proc. EAGE 63rd Conference and Technical Exhibition*, Amsterdam, The Netherlands, 4p.
- Hugenschmidt, J. (2002), "Concrete bridge inspection with a mobile GPR system," *Construction and Building Materials* Vol. 16, No. 3, 147-154.
- Krause, M., Maierhofer, C. and Wiggenhauser, H. (1995), "Thickness measurement of concrete elements using radar and ultrasonic impulse echo techniques," *Proc. 6th Int. Conf. Structural Faults and Repair*, London, UK, 17-24.

- Lualdi, M., Zanzi, L. and Binda, L. (2003), "Acquisition and processing requirements for high quality 3D reconstructions from GPR investigations," *Proc. International Symposium Non-Destructive Testing in Civil Engineering (NDT-CE)*,Berlin ,Germany, CDROM.
- Maierhofer, Ch., Brink, A., Röllig, M. and Wiggenhauser, M. (2003), "Detection of shallow voids in concrete structures with impulse thermography and radar," *NDT&E International*, Vol. 36, No. 4, 257-263.
- Valle, S., Zanzi, L. and Lenzi, G. (2000), "2D and 3D focusing of ground penetrating radar data for NDT," *Proc. 8th International Conference on Ground Penetrating Radar*, 157-162.
- Valle, S., Zanzi, L. and Rocca, F. (1999), "Radar tomography for NDT: comparison of techniques," *Journal of Applied Geophysics*, Vol. 41, No. 2-3, 259-269.